Machine Learning in Spectral CT

Hengyong Yu, PhD

University of Massachusetts Lowell

1/21/2020

Outline

1. Introduction
2. Model & Optimization
3. Experiment results
4. Discussion & Conclusion

Introduction

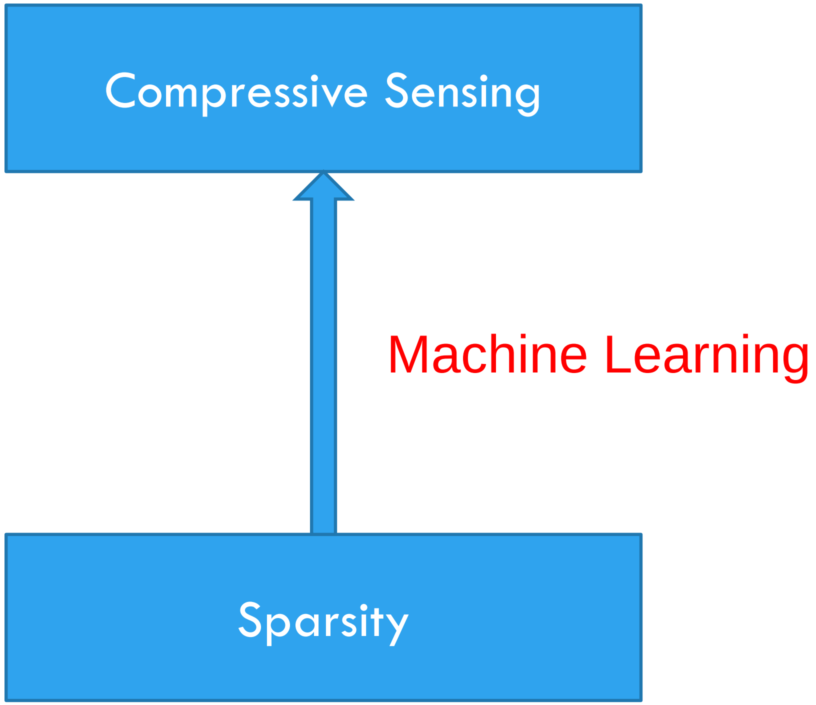

To apply the CS technique in the CT field, the key is to explore the sparsity in a transform domain, and machine learning plays an important role for this goal.

Introduction

2009 We developed the CS-based interior tomography theory and algorithms to solve the long-standing “interior problem” for high-fidelity local reconstruction

IOP PUBLISHING PHYSICS IN MEDICINE AND BIOLOGY

Phys. Med. Biol. **54** (2009) 2791–2805 doi:10.1088/0031-9155/54/9/014

Compressed sensing based interior tomography

Hengyong Yu and Ge Wang

Biomedical Imaging Division, VT-WFU School of Biomedical Engineering and Science, Virginia Tech, Blacksburg, VA 24061, USA

E-mail: hengyong-yu@ieee.org and ge-wang@ieee.org

Received 7 January 2009, in final form 13 March 2009
Published 15 April 2009
Online at stacks.iop.org/PMB/54/2791

Abstract
While conventional wisdom is that the interior problem does not have a unique solution, by analytic continuation we recently showed that the interior problem

Introduction

2012 We applied the dictionary learning technique for low-dose CT reconstruction.

1682 IEEE TRANSACTIONS ON MEDICAL IMAGING, VOL. 31, NO. 9, SEPTEMBER 2012

Low-Dose X-ray CT Reconstruction via Dictionary Learning

Qiong Xu, Hengyong Yu*, *Senior Member, IEEE*, Xuanqin Mou*, Lei Zhang, *Member, IEEE*, Jiang Hsieh, *Senior Member, IEEE*, and Ge Wang, *Fellow, IEEE*

***Abstract*—Although diagnostic medical imaging provides enormous benefits in the early detection and accuracy diagnosis of various diseases, there are growing concerns on the potential side effect of radiation induced genetic, cancerous and other diseases. How to reduce radiation dose while maintaining the diagnostic performance is a major challenge in the computed tomography (CT) field. Inspired by the compressive sensing theory, the sparse constraint in terms of total variation (TV) minimization has already better images with lower noise and more detailed structural features in our selected cases. However, there is no proof that this is true for all kinds of structures.**

***Index Terms*—Compressive sensing (CS), computed tomography (CT), dictionary learning, low-dose CT, sparse representation, statistical iterative reconstruction.**

Introduction

2013 Learning based method for imaging biomarkers

Funded Project (NIH/NIBIB R21 EB019074)

Proposal first submission date: Nov. 2013,

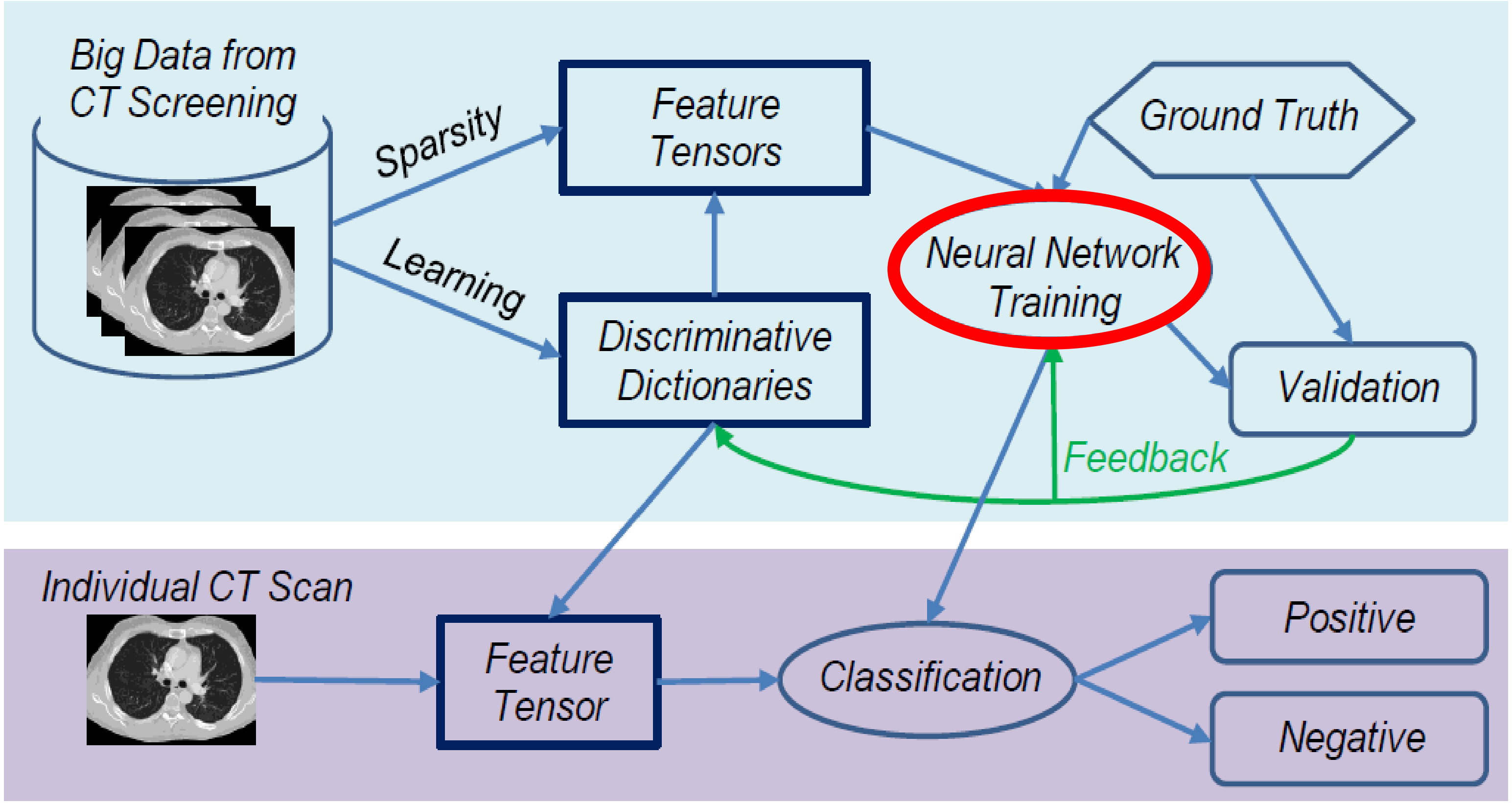

Introduction

2017

142 IEEE TRANSACTIONS ON MEDICAL IMAGING, VOL. 36, NO. 1, JANUARY 2017

Tensor-Based Dictionary Learning for Spectral CT Reconstruction

Yanbo Zhang, *Member, IEEE*, Xuanqin Mou*, *Member, IEEE*, Ge Wang, *Fellow, IEEE*,
and Hengyong Yu*, *Senior Member, IEEE*

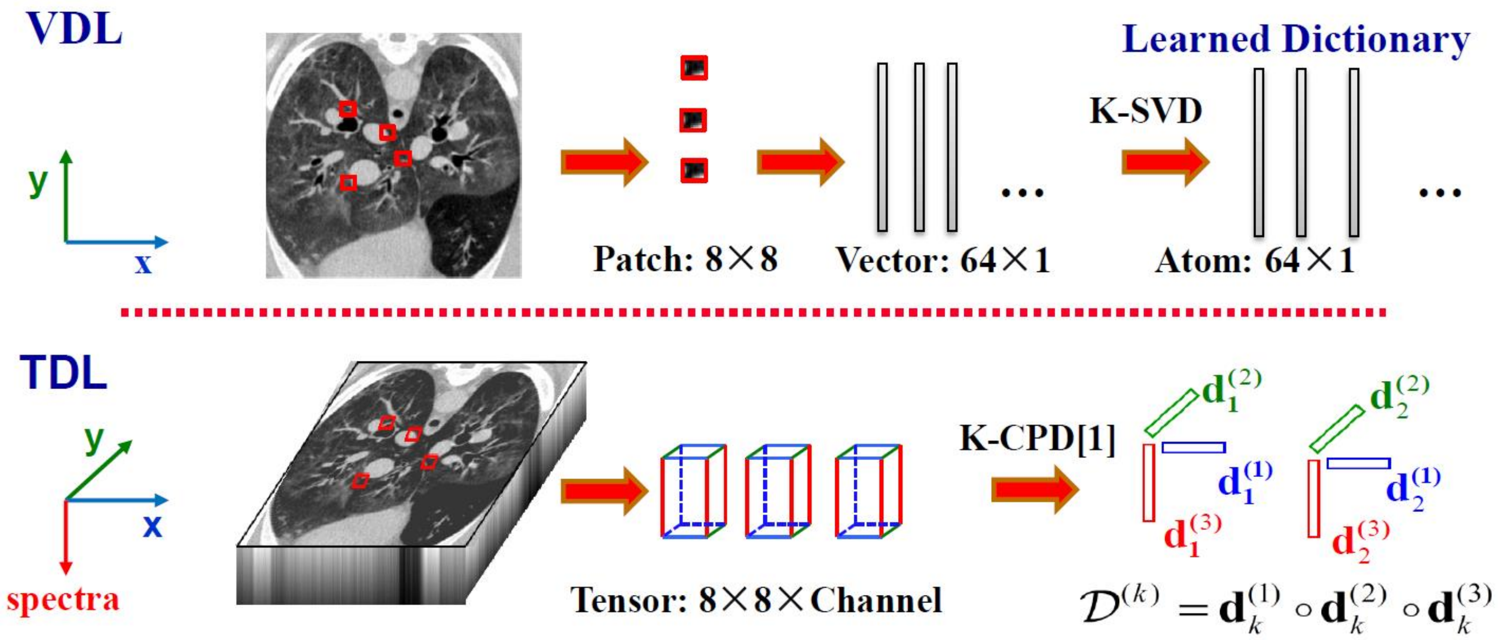

Introduction

2018

1370 IEEE TRANSACTIONS ON MEDICAL IMAGING, VOL. 37, NO. 6, JUNE 2018

Convolutional Neural Network Based Metal Artifact Reduction in X-Ray Computed Tomography

Yanbo Zhang, *Senior Member, IEEE*, and Hengyong Yu, *Senior Member, IEEE*

Workflow of The Proposed CNN-MAR

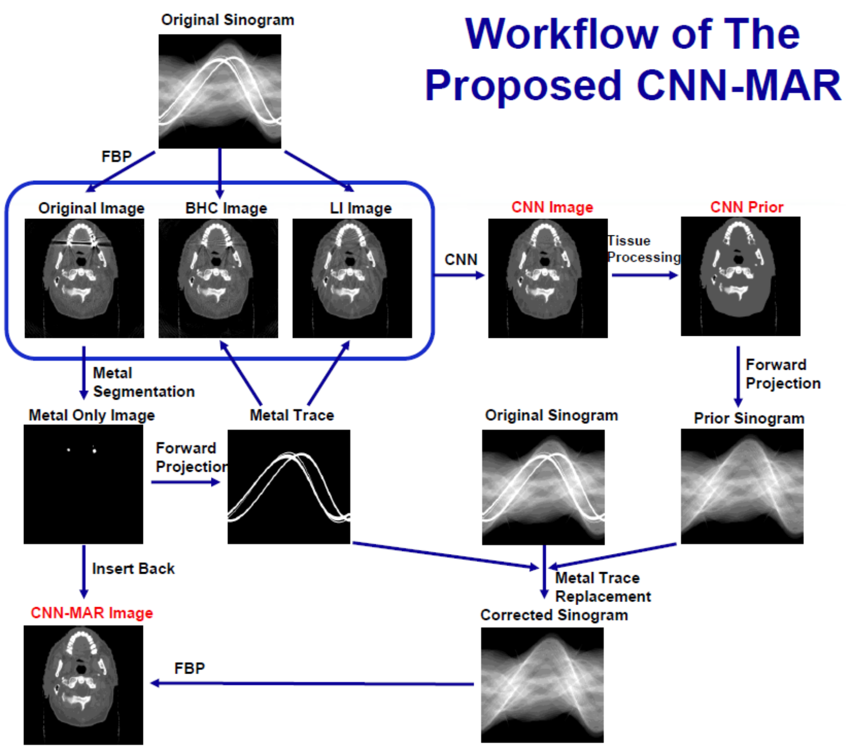

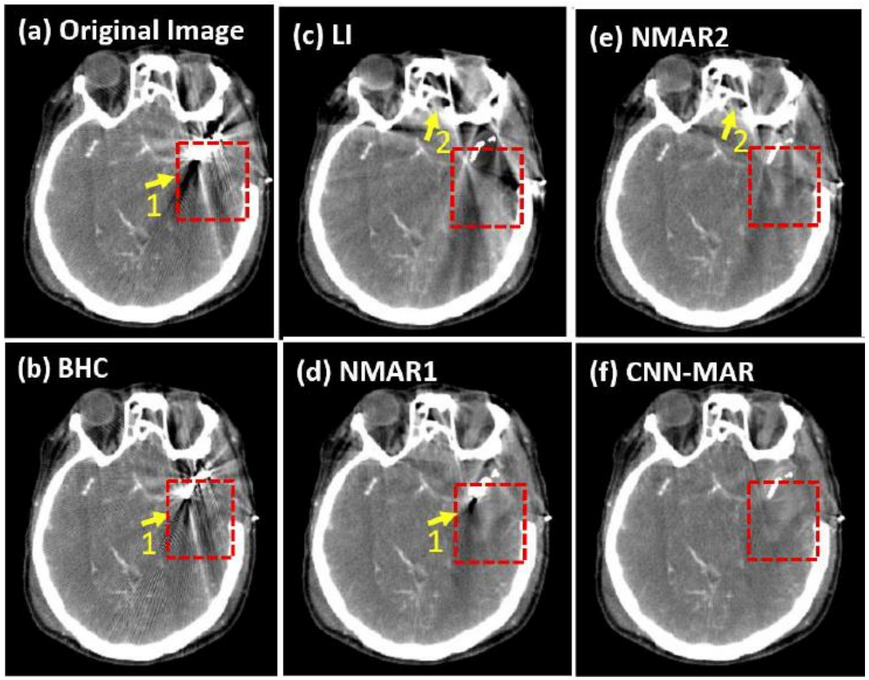

Introduction

2019

IEEE TRANSACTIONS ON MEDICAL IMAGING, VOL. 38, NO. 4, APRIL 2019 1079

Non-Local Low-Rank Cube-Based Tensor Factorization for Spectral CT Reconstruction

Weiwen Wu, Fenglin Liu, Yanbo Zhang, *Senior Member, IEEE*, Qian Wang, and Hengyong Yu, *Senior Member, IEEE*

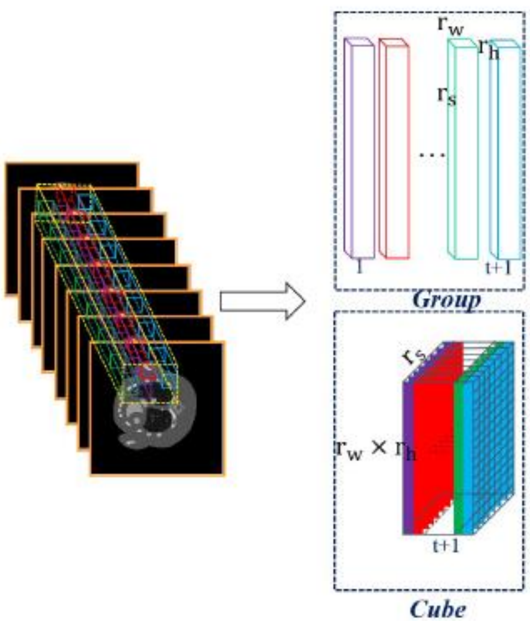

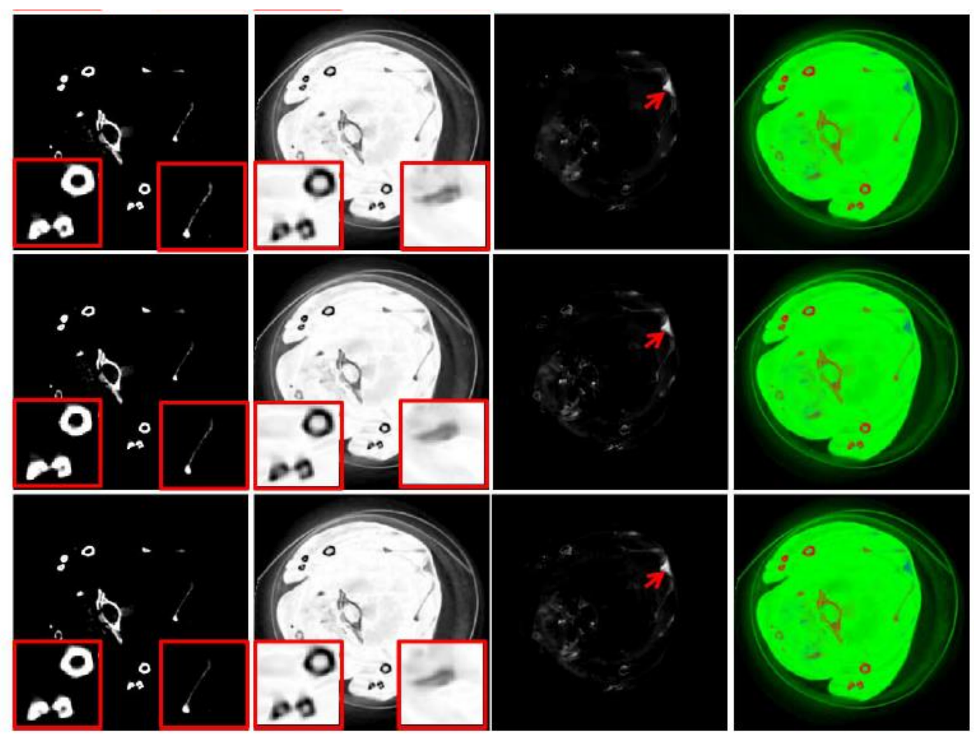

Introduction

Focus of this talk (Under Review)

Dictionary Learning based Image-domain Material Decomposition for spectral CT

Weiwen Wu[1], Haijun Yu[1], Peijun Chen[1], Fulin Luo[2], Fenglin Liu[1,3,*], Qian Wang[4], Yining Zhu[5], Yanbo Zhang[4], Jian Feng[1] and Hengyong Yu[4,*]

[1]Key Lab of Optoelectronic Technology and Systems, Ministry of Education, Chongqing University, Chongqing 400044, China
[2]State Key Laboratory of Information Engineering in Surveying, Mapping and Remote Sensing, Wuhan University, Wuhan 430079, China
[3]Engineering Research Center of Industrial Computed Tomography Nondestructive Testing, Ministry of Education, Chongqing University, Chongqing 400044, China
[4]Department of Electrical and Computer Engineering, University of Massachusetts Lowell, Lowell, MA 01854, USA
[5]School of Mathematical Sciences, Capital Normal University, Beijing, 100048, China
*Corresponding author: Fenglin Liu and Hengyong Yu
E-mail: liufl@cqu.edu.cn and hengyong-yu@ieee.org .

Introduction

Material decomposition:

I. Direct material decomposition methods: directly obtain material components using x-ray spectrum from projections

Pros:

- **Avoid the x-ray beam hardening artifacts;**
- **Regularization prior can penalize material maps;**

Cons:

- **The real x-ray spectrum is difficult to achieved;**
- **Projection noise can be amplified in projection decomposition;**

II. Indirect material decomposition methods: including projection-based and image-based methods

Pros:

- **The regularization prior can penalize projections or reconstructed map images;**
- **Image-based methods can reduce noise well;**

Pros:

- **Cannot avoid x-ray beam hardening artifacts;**

Introduction

Material decomposition methods:

Spectral CT images (attenuation maps at from all energy bins) are available using image reconstruction methods (such as FBP, etc)

- Conventional image-domain decomposition
  - Direct matrix inversion decomposition[4]

    Sensitive to artifacts and noise.
  - Regularized (model-based) decomposition

    Statistical measurement model + Object prior model

    Improves image quality and decomposition accuracy

[4] [Zhang et al., IEEE T-MI, 2016]

Introduction

Regularization methods for material decomposition:

- Material decomposition with prior knowledge aware iterative denoising (MD-PKAID) [5]
  - Retain structure details by exploring the structural redundancy
  - The material accuracy and image quality depending on prior image
- Density, local joint Sparsity and structural low-Rank (DSR) [6]
  - Artifact reduction with improvement of material accuracy
  - Ignores the physical effects with many parameters
  - Validate only on numerical phantom

[5] [Tao et al., Physical in medicine and biology, 2018]

[6] [Xie et al., Journal of Nondestructive Evaluation, 2019]

Outline

- 1. Introduction
- **2. Model & Optimization**
- 3. Experiment results
- 4. Discussion & Conclusion

Model formulation

Material decomposition basic model[7]

$$\begin{bmatrix} \vartheta_{11} & \cdots & \vartheta_{1M} \\ \vdots & \ddots & \vdots \\ \vartheta_{N1} & \cdots & \vartheta_{NM} \end{bmatrix} \begin{bmatrix} \boldsymbol{f}_1 \\ \vdots \\ \boldsymbol{f}_M \end{bmatrix} = \begin{bmatrix} \overline{\boldsymbol{x}_1} \\ \vdots \\ \overline{\boldsymbol{x}_N} \end{bmatrix} \tag{1}$$

- $\vartheta_{nm}(1 \le n \le N, 1 \le m \le M)$------ averaged attenuation coefficients of the mth material at nth energy window;
- $\boldsymbol{f}_m(1 \le m \le M)$------ m^{th} material component maps;
- $\overline{\boldsymbol{x}_n}(1 \le n \le N)$ ------ spectral CT image of the n^{th} energy window.

The matrix form of Eq. (1) can be formulated as

$$\vartheta \mathcal{F}_{(3)} = \mathcal{X}_{(3)} \tag{2}$$

- $\boldsymbol{\vartheta} = \begin{bmatrix} \vartheta_{11} & \cdots & \vartheta_{1M} \\ \vdots & \ddots & \vdots \\ \vartheta_{N1} & \cdots & \vartheta_{NM} \end{bmatrix} \in \mathcal{R}^{N\times M}$; .
- $\mathcal{F} \in \mathcal{R}^{J_1\times J_2\times M}$ and $\mathcal{X} \in \mathcal{R}^{J_1\times J_2\times N}$ represent two tensors;
- $\mathcal{F}_{(3)} \in \mathcal{R}^{M\times J}$ $(J = J_1 \times J_2)$ and $\mathcal{X}_{(3)} \in \mathcal{R}^{N\times J}$ are the mode-3 unfolding of $\mathcal{F}$ and $\mathcal{X}$.

[7] [Wu et al., Arxiv, 2019]
[8] [Wu et al, IEEE Access, 2019]

Model formulation

Considering noise in the reconstructed images, Eq. (2) can be read as

$$\vartheta \mathcal{F}_{(3)} = \boldsymbol{\mathcal{X}}_{(3)} + \boldsymbol{\eta} \qquad (3)$$

- $\boldsymbol{\eta}$ ------the noise level

$$argmin\left(\frac{1}{2}\left\|\boldsymbol{\mathcal{X}}_{(3)} - \vartheta \mathcal{F}_{(3)}\right\|_{\boldsymbol{F}}^{2} + \lambda R\left(\mathcal{F}\right)\right) \qquad (4)$$

- $R(\mathcal{F})$------ the regularization term
- λ ------the regularized parameter

$R(\mathcal{F})$ can be the Total Variation (TV), non-local mean and block matching frame and so on.

[7] [Wu et al., Arxiv, 2019]

Model formulation

The idea of vectoried dictionary learning (DL):

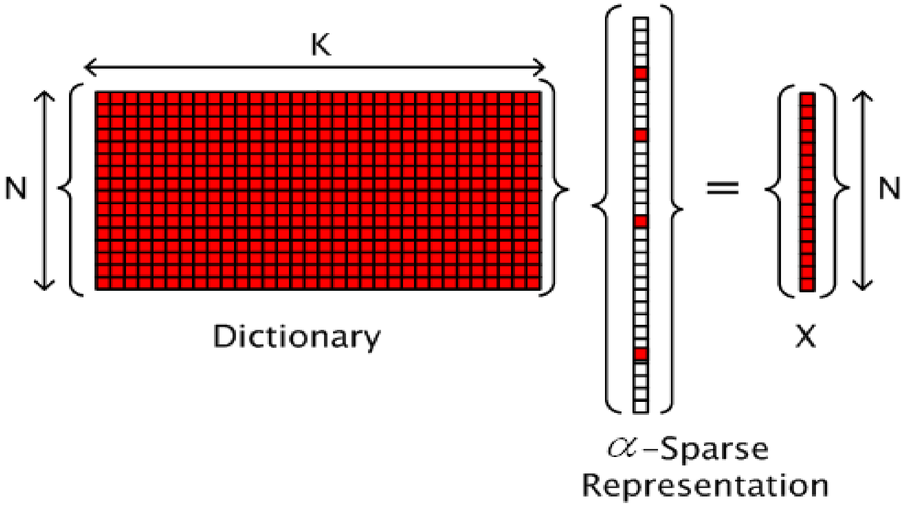

Dictionary $\mathbf{D} \in R^{N \times K}, N \ll K$

Image patch $\mathbf{x} \in R^{N \times 1}$

Sparse representation

$\boldsymbol{\alpha} \in R^{K \times 1}, \ \|\boldsymbol{\alpha}\|_0 = N = K$

$$\boxed{\min_{\boldsymbol{\alpha}} \|\boldsymbol{\alpha}\|_0 \quad s.t. \quad \|\mathbf{x} - \mathbf{D}\boldsymbol{\alpha}\|_2^2 \le \varepsilon}$$

Given a training set of patches, $\mathbf{x}_s \in R^{N \times 1}, (s = 1, \ldots, S)$, the dictionary learning is to solve

$$\boxed{\min_{\mathbf{D}, \boldsymbol{\alpha}} \sum_{s=1}^{S} \left(\|\mathbf{x}_s - \mathbf{D}\boldsymbol{\alpha}_s\|_2^2 + \nu_s \|\boldsymbol{\alpha}_s\|_0 \right)}$$

Model formulation

The conventional dictionary learning based image-domain material decomposition can be expressed as

$$\underset{\mathcal{F},\{\boldsymbol{\beta}_m\}_{m=1}^{M}}{argmin} \left(\boxed{\frac{1}{2}\left\| \mathcal{X}_{(3)} - \vartheta \mathcal{F}_{(3)} \right\|_F^2} + \boxed{\sum_{m=1}^{M} \frac{\lambda_m}{2} \sum_{i=1}^{I} \left(\left\| \mathcal{H}_i(\boldsymbol{F}_m) - \mathbf{D}_m \boldsymbol{\beta}_{mi} \right\|_F^2 + v_{mi} \left\| \boldsymbol{\beta}_{mi} \right\|_0 \right)} \right) \quad (5)$$

The data fidelity term

Dictionary learning regularization term

- $\boldsymbol{F}_m$------ m^{th} channel of material images $\mathcal{F}$
- $\boldsymbol{\beta}_{mi} \in \mathcal{R}^{T\times 1}$------sparse representation coefficients for i^{th} image patch from m^{th} material image
- $\boldsymbol{\beta}_m = \{\boldsymbol{\beta}_{mi}\}_{i=1}^{I}$
- $\mathcal{H}_i(\boldsymbol{F}_m)$------the i^{th} image patch extraction operator from $\boldsymbol{F}_m$
- $\boldsymbol{D}_m$------the trained dictionary for m^{th} material
- $\boldsymbol{\lambda}_m$------the regularized parameter for m^{th} material

[7] [Wu et al., Arxiv, 2019]

Model formulation

Cons of conventional dictionary learning based image-domain material decomposition:

- Because a specific material map may only contain a few image features, it is difficult for the trained $\boldsymbol{D}_m$ to encode the image features and reduce sparse level;
- training different $\boldsymbol{D}_m$ is time consuming;
- the correlation between different material maps will be lost

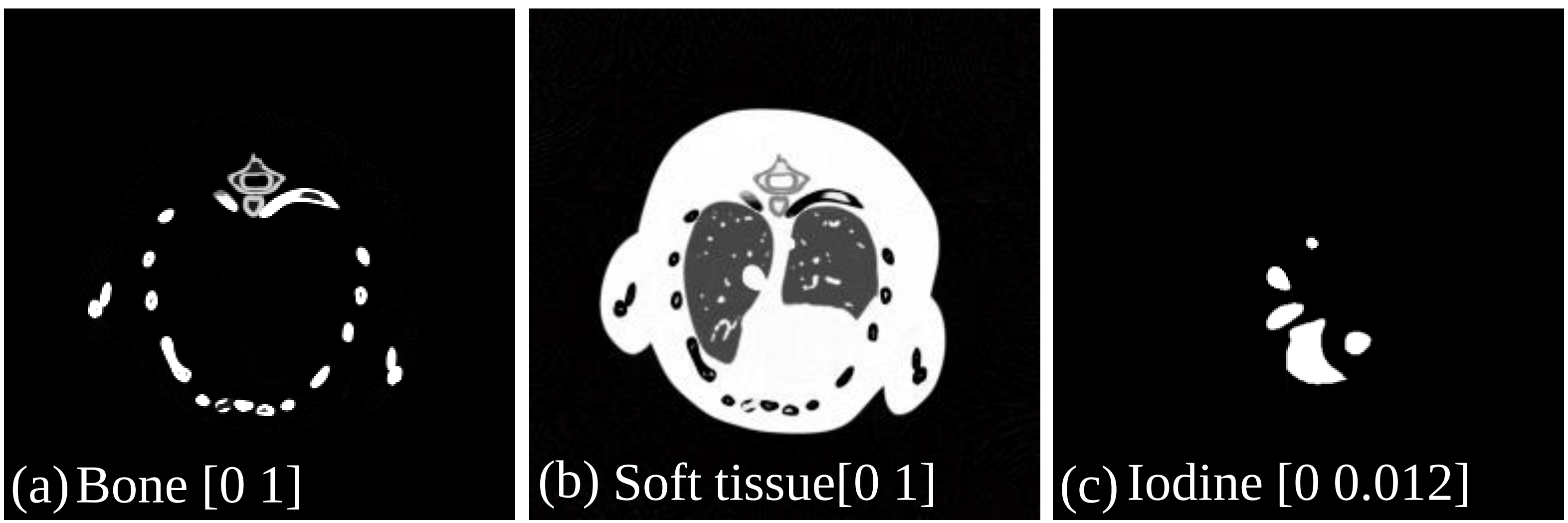

Three basis materials of numerical mouse

[7] [Wu et al., Arxiv, 2019]

Model formulation

Solution

- Training a unified dictionary using image patches from all material images;
- The normalization strategy is operated on the training material image to avoid the data inconsistency of material images;

The conventional dictionary learning based image-domain material decomposition can be expressed as

$$\underset{\mathcal{F},\{\boldsymbol{\beta}_m\}_{m=1}^{M}}{\arg\min}\left(\frac{1}{2}\left\|\boldsymbol{\mathcal{X}}_{(3)}-\vartheta\boldsymbol{\mathcal{F}}_{(3)}\right\|_F^2+\sum_{m=1}^{M}\frac{\lambda_m}{2}\sum_{i=1}^{I}\left(\left\|\mathcal{H}_i\left(\boldsymbol{F}_m\right)-\boldsymbol{D}\boldsymbol{\beta}_{mi}\right\|_F^2+v_{mi}\left\|\boldsymbol{\beta}_{mi}\right\|_0\right)\right) \quad (6)$$

The data fidelity term

Dictionary learning regularization term

- $\hat{\boldsymbol{D}}$------the trained unified dictionary

[7] [Wu et al., Arxiv, 2019]

Model formulation

Additional conditions

① If the air is also treated as one basis material, the summation of pixel values of different material images at the same location should be equal to one, i.e.,

$$\left(\sum_{m=1}^{M}\mathcal{F}_{j_1 j_2 m}\right)+\boldsymbol{AIR}_{j_1 j_2}=1\left(1\leq j_1\leq J_1, 1\leq j_2\leq J_2\right) \quad (7)$$

- $\boldsymbol{AIR}$ is the air map and $\boldsymbol{AIR}_{j_1 j_2}$ represents the binary pixel value at $(j_1, j_2)^{th}$ location. A threshold method is applied to determine the air map (0 or 1).

② The pixel value within $\boldsymbol{\mathcal{F}}$ should be in the range of [0 1],i.e.,

$$0\leq\mathcal{F}_{j_1 j_2 m}\leq 1. \quad (8)$$

[7] [Wu et al., Arxiv, 2019]

Model formulation

Considering Eqs. (7) and (8), the proposed dictionary learning based image-domain material decomposition (DLIMD) method can be formulated as

$$\underset{\mathcal{F},\{\boldsymbol{\beta}_m\}_{m=1}^{M}}{argmin}\left(\frac{1}{2}\left\|\mathcal{X}_{(3)}-\vartheta\mathcal{F}_{(3)}\right\|_{\boldsymbol{F}}^{2}+\sum_{m=1}^{M}\frac{\lambda_m}{2}\sum_{i=1}^{I}\left(\left\|\mathcal{H}_i\left(\boldsymbol{F}_m\right)-\boldsymbol{D}\boldsymbol{\beta}_{mi}\right\|_{F}^{2}+v_{mi}\left\|\boldsymbol{\beta}_{mi}\right\|_0\right)\right)$$
$$s.t.\left(\sum_{m=1}^{M}\mathcal{F}_{j_1j_2m}\right)+\boldsymbol{AIR}_{j_1j_2}=1,\forall j_1,j_2,0\le\mathcal{F}\le1. \tag{9}$$

Pros:

- can fully encode similarities within different material images;
- can enhance the redundancy with the trained dictionary $\widehat{\mathbf{D}}$;
- save training time to some extent in practice.

[7] [Wu et al., Arxiv, 2019]

Optimization

Introducing tensor $\boldsymbol{\mathcal{U}}$ to replace $\boldsymbol{\mathcal{F}}$, Eq. (9) can be converted into

$$\underset{\mathcal{F},\{\boldsymbol{\beta}_m\}_{m=1}^{M},\mathcal{U}}{argmin}\left(\frac{1}{2}\left\|\mathcal{X}_{(3)}-\vartheta\mathcal{F}_{(3)}\right\|_{\boldsymbol{F}}^{2}+\sum_{m=1}^{M}\frac{\lambda_m}{2}\sum_{i=1}^{I}\left(\left\|\mathcal{H}_i\left(\boldsymbol{U}_m\right)-\boldsymbol{D}\boldsymbol{\beta}_{mi}\right\|_F^2+v_{mi}\left\|\boldsymbol{\beta}_{mi}\right\|_0\right)\right) \quad (10)$$

$$s.t.\left(\sum_{m=1}^{M}\mathcal{F}_{j_1 j_2 m}\right)+\boldsymbol{AIR}_{j_1 j_2}=1,\forall j_1,j_2,\mathcal{U}=\mathcal{F},0\le\mathcal{F}\le 1.$$

Eq. (10) can be divided into two sub-problem

$$\begin{cases}\underset{\mathcal{F}}{argmin}\left(\frac{1}{2}\left\|\mathcal{X}_{(3)}-\vartheta\mathcal{F}_{(3)}\right\|_F^2+\frac{\eta}{2}\left\|\mathcal{F}-\mathcal{U}^{(k)}\right\|_F^2\right) \\ s.t.\left(\sum_{m=1}^{M}\mathcal{F}_{j_1 j_2 m}\right)+AIR_{j_1 j_2}=1,\forall j_1,j_2,0\le\mathcal{F}\le 1. \quad (11a) \\ \underset{\mathcal{U},\{\boldsymbol{\beta}_m\}_{m=1}^{M}}{arg\,min}\left(\frac{\eta}{2}\left\|\mathcal{U}-\mathcal{F}^{(k+1)}\right\|_F^2+\sum_{m=1}^{M}\frac{\lambda_m}{2}\sum_{i=1}^{I}\left(\left\|\mathcal{H}_i\left(\mathbf{U}_m\right)-\hat{\mathbf{D}}\boldsymbol{\beta}_{mi}\right\|_F^2+v_{mi}\left\|\boldsymbol{\beta}_{mi}\right\|_0\right)\right) \quad (11b)\end{cases}$$

[7] [Wu et al., Arxiv, 2019]

Optimization

As for Eq. (11a), it can be simplified as[7]

$$\underset{\mathcal{F}_{j_1 j_2 \#}}{argmin} \frac{1}{2}\left\| \left(\vartheta^{\mathrm{T}}\vartheta + \eta \mathbf{I}\right)\mathcal{F}_{j_1 j_2 \#} - \left(\vartheta^{\mathrm{T}}\boldsymbol{\mathcal{X}}_{\# j_1 j_2} + \eta \boldsymbol{\mathcal{U}}^{(k)}_{j_1 j_2 \#}\right)\right\|_F^2 \tag{12}$$

$$\forall j_1, j_2, s.t. \left(\sum_{m=1}^{M} \mathcal{F}_{j_1 j_2 m}\right) = 1, 0 \le \mathcal{F}_{j_1 j_2 \#} \le 1.$$

Eq. (12) is a constrained least square problem and it can be easily solved.

For Eq. (11b) can be divided into the following problem

$$\underset{\mathbf{U}_m, \boldsymbol{\beta}_m}{argmin} \frac{1}{2}\left\|\mathbf{U}_m - \mathbf{F}_m^{(k+1)}\right\|_F^2 + \frac{\tau_m}{2}\sum_{i=1}^{I}\left(\left\|\mathcal{H}_i\left(\mathbf{U}_m\right) - \hat{\mathbf{D}}\boldsymbol{\beta}_{mi}^{(k+1)}\right\|_F^2 + v_{mi}\left\|\boldsymbol{\beta}_{mi}\right\|_0\right), 1 \le m \le M \tag{13}$$

where $\tau_m = \lambda_m/\eta$, the Eq. (13) can be solved by using the method in [8]

[7] [Wu et al., Arxiv, 2019]
[9] [Wu et al., APM, 2018]

Outline

1. Introduction

2. Model & Optimization

3. Experiment results

4. Discussion & Conclusion

Implementation

- Comparisons: Direct inversion (DI) method, total variation material decomposition (TVMD) method
- The iteration number is 30 and the parameters in Table I
- The number of atoms within the dictionary are set as 512 and Image patches are 10000, patch stride 1×1
- Other parameters are in the following Table

Parameters	η	L	Patch Size	$\varepsilon_{\mathrm{Al/bone,Water/Tisuue,Iodine/GNP}}$
Numerical mouse	3×10^{-5}	3	10x10	(0.02, 0.057, 0.0025)
Physical phantom	0.003	10	8x8	(0.08, 0.03, 0.0025)
Preclinical experiment	0.001	12	8x8	(0.004,0.012,0.05)

[7] [Wu et al., Arxiv, 2018]

Implementation

- Three indexes, i.e., RMSE, PSNR and SSIM are employed
- The unified dictionaries used in numerical mouse, physical phantom and preclinical experiment

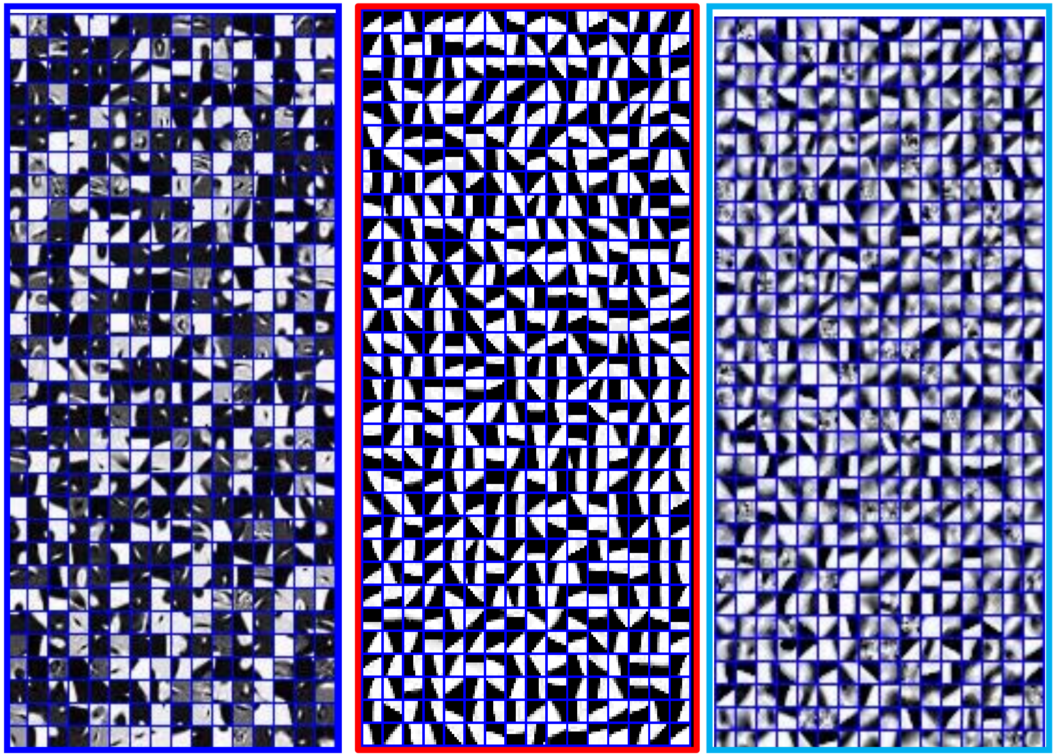

The dictionaries are trained from DI results of numerical mouse, physical phantom and preclinical experiment

[7] [Wu et al., Arxiv, 2018]

Section I: Numerical mouse

Material decomposition from FBP mouse results

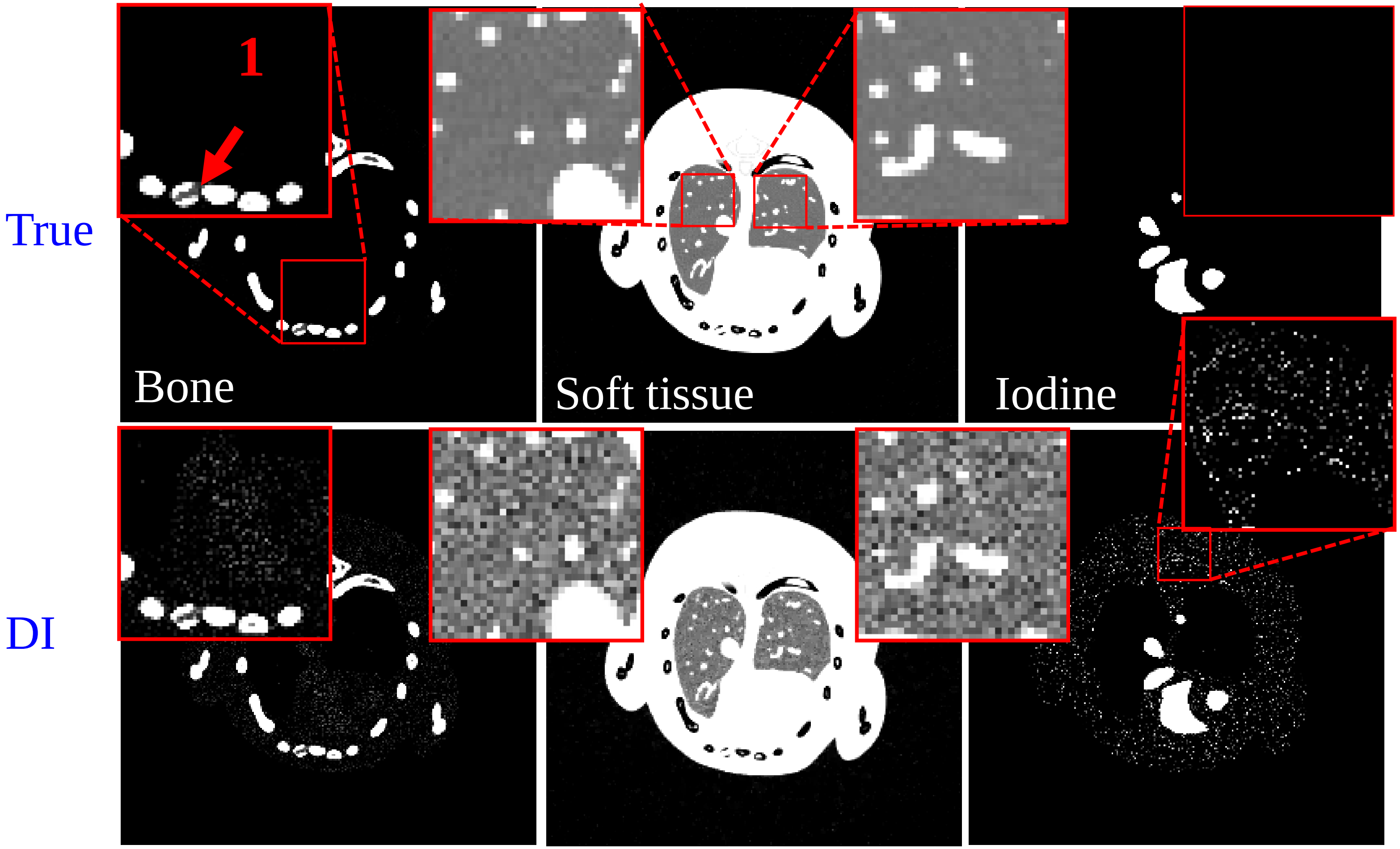

The display windows of 1st-3rd columns are [0.01, 0.2], [0.25 0.55] and [0.0007 0.003]

Section I: Numerical mouse

Material decomposition from FBP mouse results

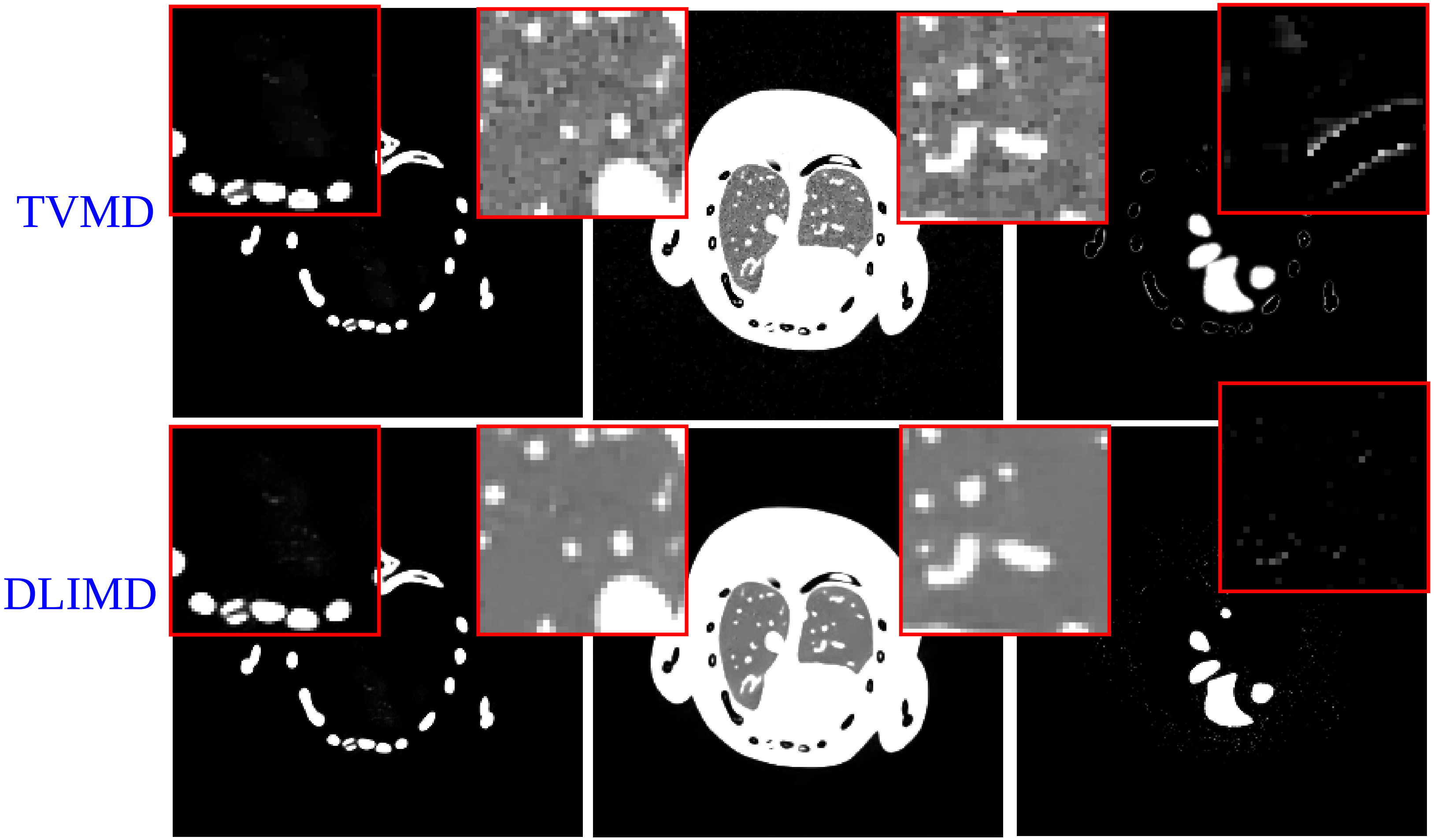

The display windows of 1st-3rd columns are [0.01, 0.2], [0.25 0.55] and [0.0007 0.003]

[8] [Wu et al., APM, 2018]

Section I: Numerical mouse

Table I. Quantitative evaluation results of three basis materials.

		RMSE(10^{-2})	PSNR	SSIM
Bone	DI	8.719	21.191	0.9314
	TVMD	8.279	21.641	0.9439
	DLIMD	**7.873**	**22.077**	**0.9461**
Soft tissue	DI	13.890	17.146	0.7834
	TVMD	12.910	17.782	0.8491
	DLIMD	**12.368**	**18.154**	**0.8646**
Iodine contrast agent	DI	0.0853	61.380	0.9056
	TVMD	0.0734	62.682	0.9214
	DLIMD	**0.0688**	**63.251**	**0.9393**

Section II: Physical phantom

Experiment set-up

- A micro-focus x-ray source (YXLON, 225Kv)
- A flat-panel PCD (Xcounter, XC-Hydra FX20)
- 2048 detector cells, 1080 views, 137kV, SOD: 182.68mm, SDD:440.50mm
- 256x256 image size

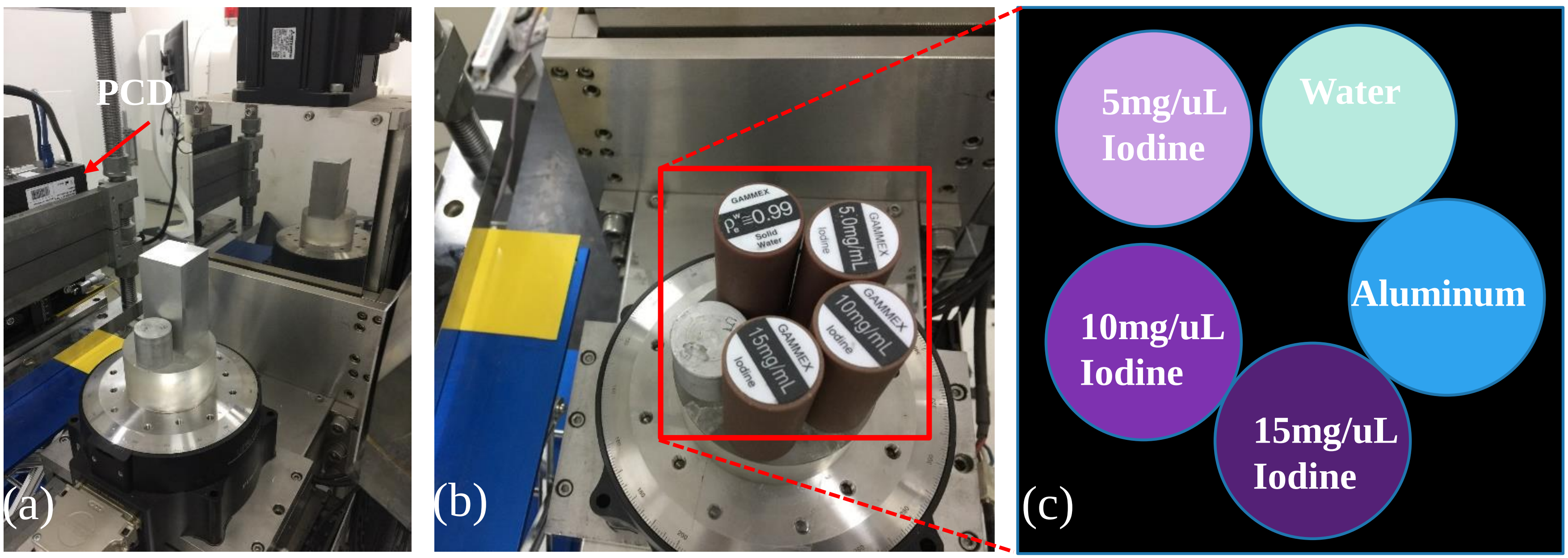

Setups of physical phantom experiments. (a) is the spectral CT system, (b) and (c) represent the physical phantom.

Section II: Physical phantom

Material decomposition results

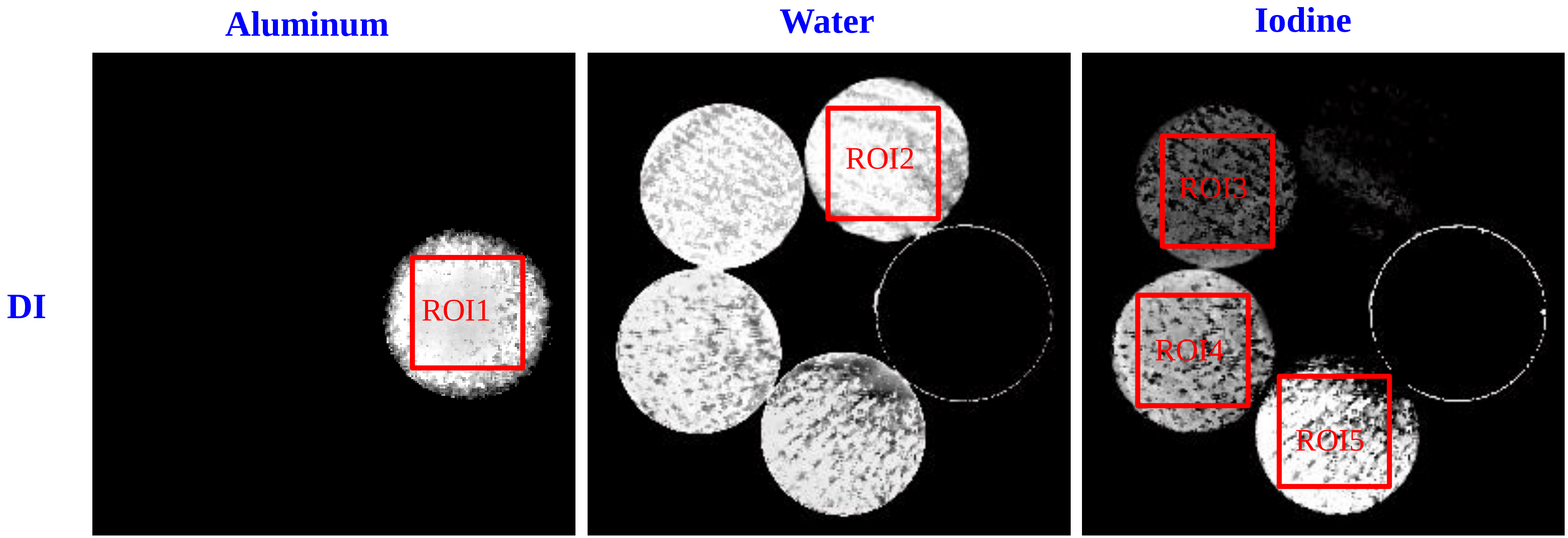

From left to right, the columns represent the decomposition results of aluminum, water and iodine, where the display windows are [0.5 1], [0.8 1] and [0 0.003].

Section II: Physical phantom

Material decomposition results

Aluminum Water Iodine

TVMD

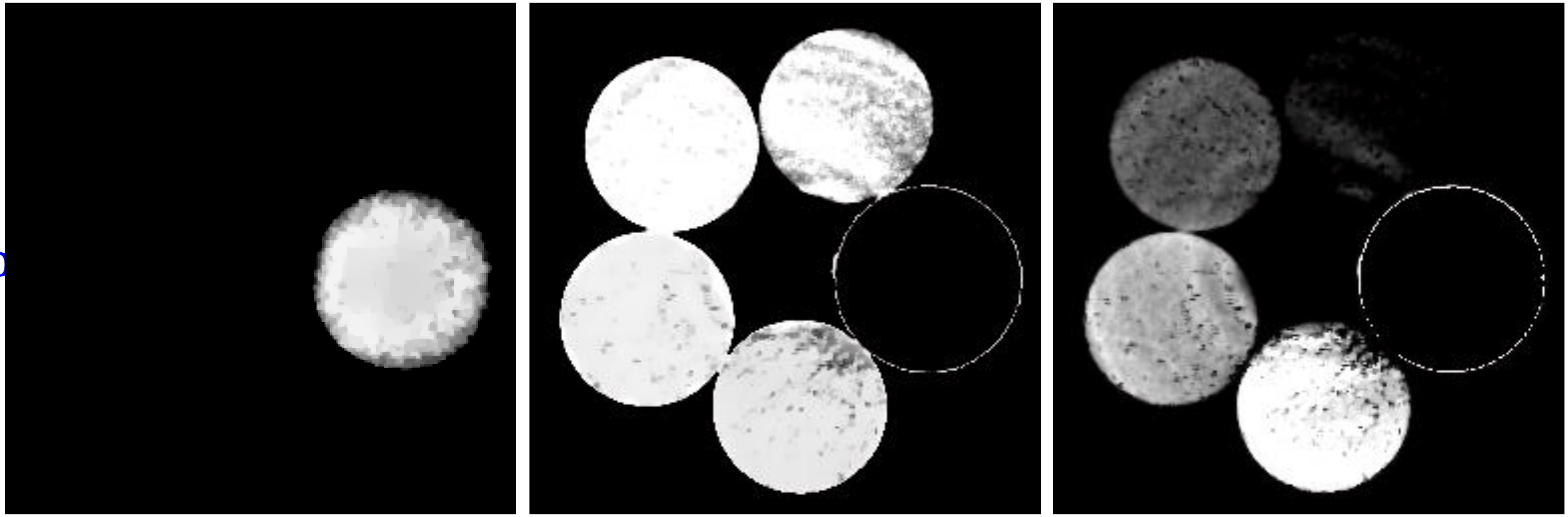

From left to right, the columns represent the decomposition results of aluminum, water and iodine, where the display windows are [0.5 1], [0.8 1] and [0 0.003].

Section II: Physical phantom

Material decomposition results

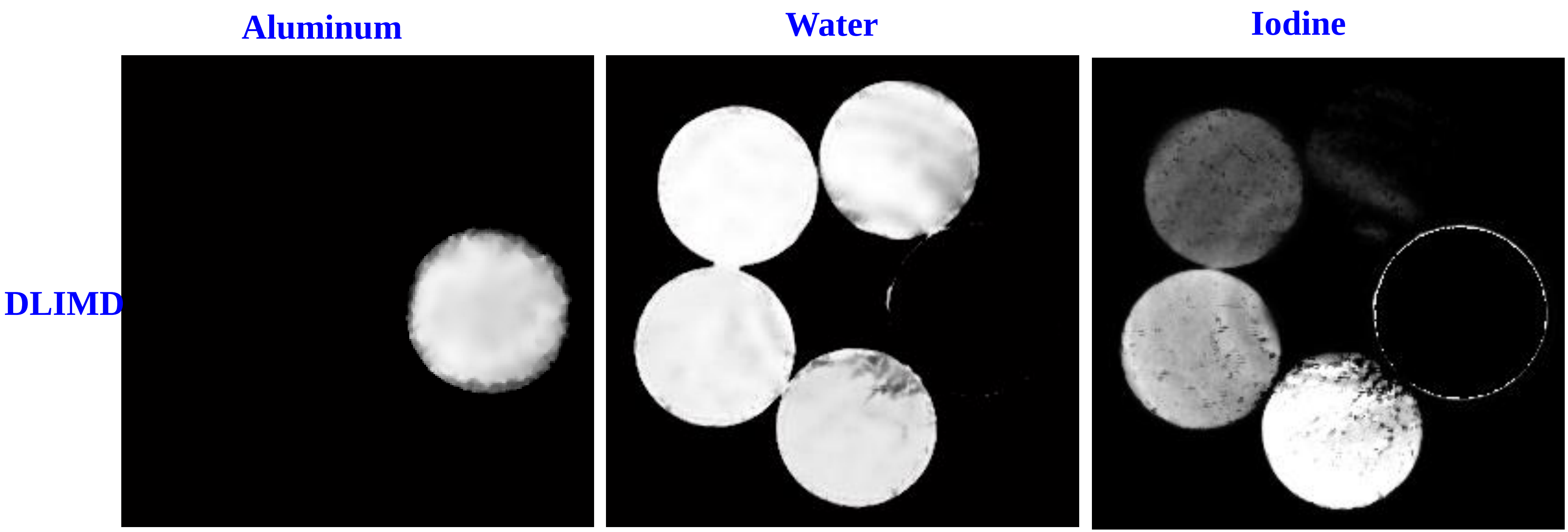

From left to right, the columns represent the decomposition results of aluminum, water and iodine, where the display windows are [0.5 1], [0.8 1] and [0 0.003].

Section II: Physical phantom

Table II. Quantitative evaluation results of ROI 1-5

		RMSE(10^{-4})	PSNR	SSIM
ROI-1	DI	889	21.026	0.9882
	TVMD	861	21.299	0.9882
	DLIMD	**828**	**21.635**	**0.9925**
ROI-2	DI	324	29.796	0.9732
	TVMD	291	30.718	0.9913
	DLIMD	**271**	**31.329**	**0.9977**
ROI-3	DI	5.253	65.593	0.4118
	TVMD	2.196	73.169	0.7588
	DLIMD	**1.812**	**74.839**	**0.8483**
ROI-4	DI	6.854	63.281	0.6200
	TVMD	3.009	70.431	0.8625
	DLIMD	**2.399**	**72.400**	**0.9165**
ROI-5	DI	12.530	58.041	0.6204
	TVMD	7.780	62.180	0.8549
	DLIMD	**7.639**	**62.340**	**0.8945**

Section III: Preclinical experiment

- PCD : PILATUS3 with 4 energy-channels by DECTRIS; It consists of 515 cells and each has a length of 0.15 mm
- Projection view is 720 and SOD= 35.27 cm, SDD= 43.58 cm
- The size of each material image is 512×512

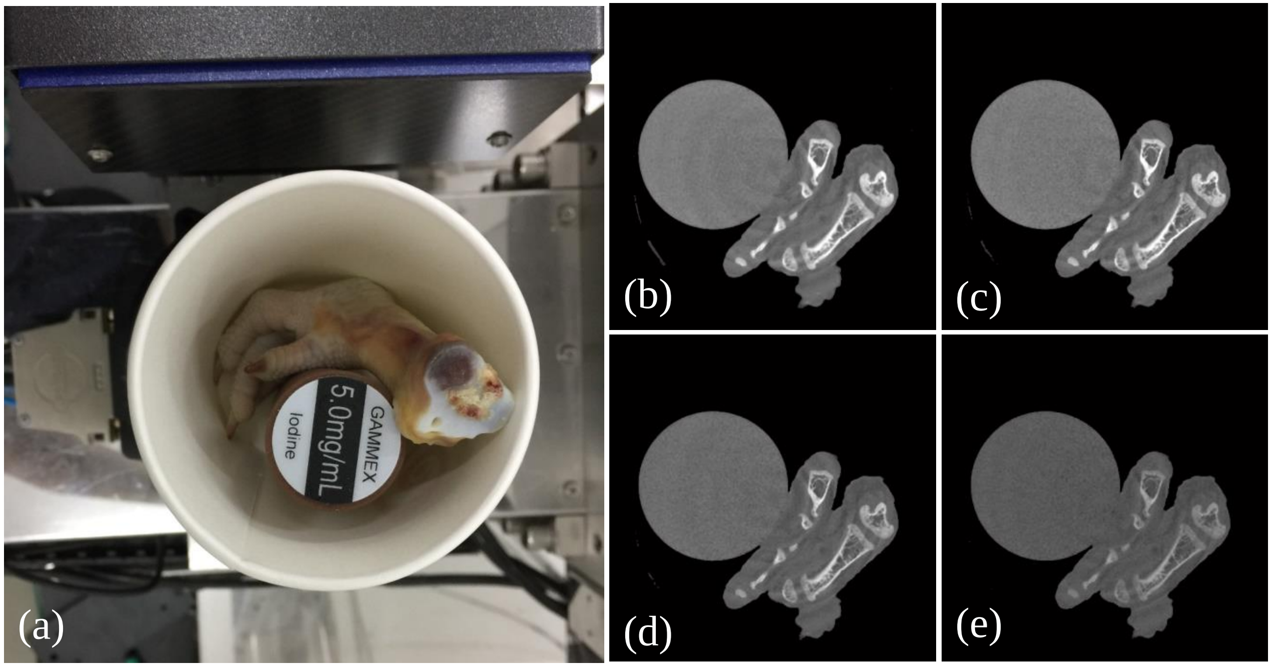

Preclinical experiment. (a) is the preclinical specimen fixed on the spectral CT system. (b)-(e) are FBP reconstruction results from 4 energy bins, where the display window is [0 0.5] cm^{-1}

Section III: Preclinical experiment

- Material decomposition results

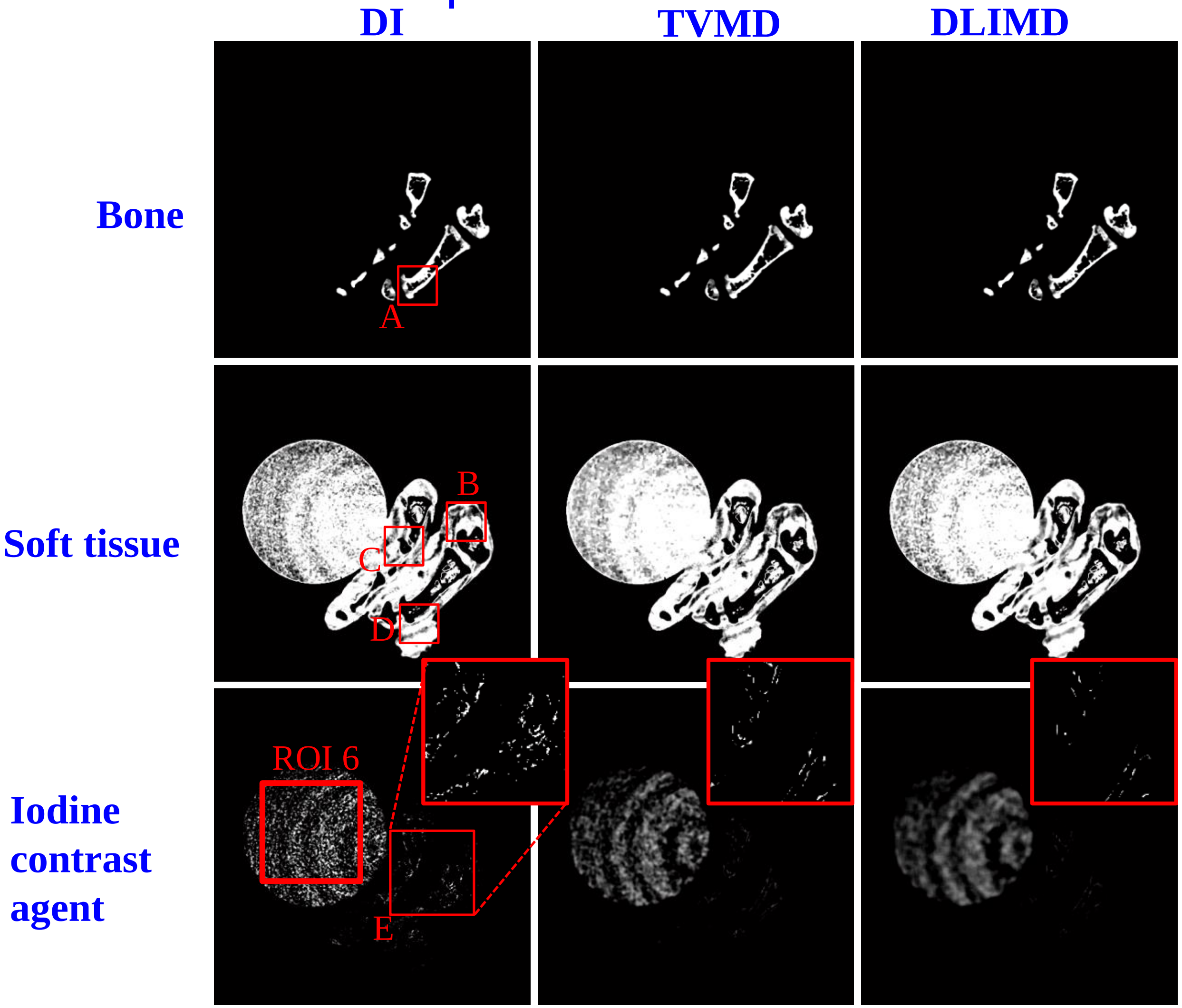

The 1st-3rd rows represent the bone, soft tissue and iodine with the display windows [0.25 0.5], [0.85 0.95] and [0.0018 0.005].

Section III: Preclinical experiment

- Material decomposition results

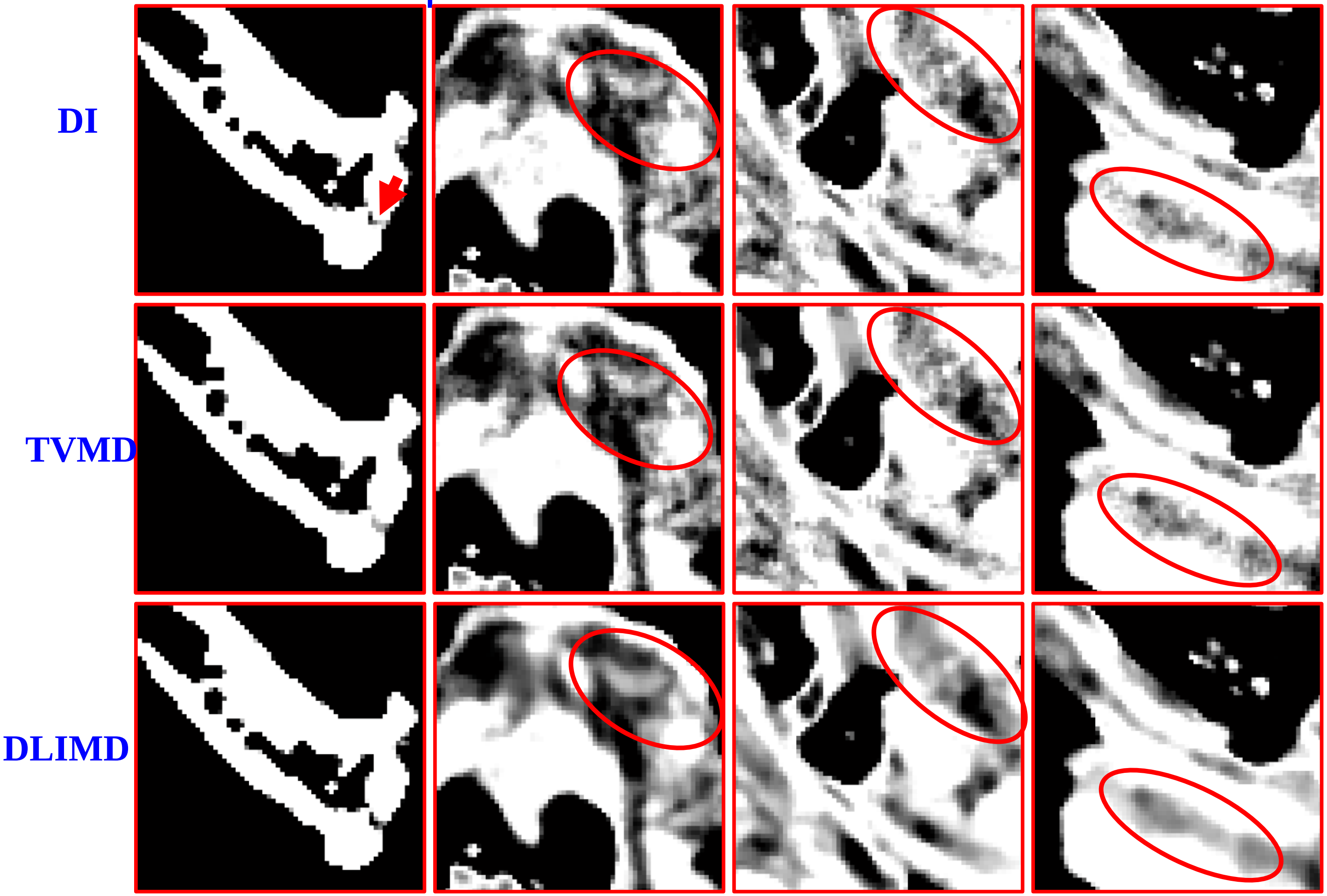

The 1st-4th rows represent the ROIs marked with “A”, “B”, “C” and “D”, where the display windows are [0.29 0.33], [0.85 0.95], [0.85 0.95] and [0.85 0.95].

Outline

1. Introduction
2. Model & Optimization
3. Experiment results
4. Discussion & Conclusion

Discussion and conclusion

- Discussion
  - Parameters are chosen empirically in the proposed DLIMD
  - The numerical mouse and two real datasets only contain three different basis materials, however the imaging objects may contain multiple (greater than 3) materials
- Conclusion
  - Considering the similarities of different material images, we construct a unified dictionary to encode material image sparsity by training a set of image patches
  - Formulating a DLIMD mathematical model by enhancing sparsity of material maps with the dictionary
  - additional constraints are incorporated into the model to further improve the decomposition accuracy

Question?